Infrared features of unquenched finite temperature lattice Landau gauge QCD

Sadataka Furui*
School of Science and Engineering, Teikyo University, 320-8551 Japan

Hideo Nakajima†
Department of Information Science, Utsunomiya University, 321-8585 Japan

(Received 10 December 2006; revised manuscript received 27 May 2007; published 24 September 2007)

The color diagonal and color antisymmetric ghost propagators slightly above T_c of $N_f = 2$ MILC $24^3 \times 12$ lattices are measured and compared with zero-temperature unquenched $N_f = 2 + 1$ MILC$_c$ $20^3 \times 64$ and MILC$_f$ $28^3 \times 96$ lattices and zero-temperature quenched 56^4 $\beta = 6.4$ and 6.45 lattices. The expectation value of the color antisymmetric ghost propagator $\phi^c(q)$ is zero, but its Binder cumulant, which is consistent with that of $N_c^2 - 1$ dimensional Gaussian distribution below T_c, decreases above T_c. Although the color diagonal ghost propagator is temperature independent, the l^1 norm of the color antisymmetric ghost propagator is temperature dependent. The expectation value of the ghost condensate observed at zero-temperature unquenched configuration is consistent with 0 in $T > T_c$. We also measure transverse, magnetic, and electric gluon propagator and extract gluon screening masses. The running coupling measured from the product of the gluon dressing function and the ghost dressing function are almost temperature independent, but the effect of A^2 condensate observed at zero temperature is consistent with 0 in $T > T_c$. The transverse gluon dressing function at low temperature has a peak in the infrared at low temperature, but it becomes flatter at high temperature. The magnetic gluon propagator at high momentum depends on the temperature. These data imply that the magnetic gluon propagator and the color antisymmetric ghost propagator are affected by the presence of dynamical quarks, and there are strong nonperturbative effects through the temperature-dependent color antisymmetric ghost propagator.

DOI: 10.1103/PhysRevD.76.054509 PACS numbers: 12.38.Gc, 11.10.Gh, 11.15.Ha, 12.38.Aw

I. INTRODUCTION

As a condition of the color confinement in the infrared region, Kugo-Ojima criterion [1] and the Gribov-Zwanziger scenario [2,3] are well known. In these theories, infrared divergence of the ghost propagator is the essential ingredient of the emergence of the stringlike interquark potential. In finite temperature SU(2) lattice Coulomb gauge simulation, linearly rising color-Coulomb potential was observed to remain above the deconfinement temperature T_c [4]. The color-Coulomb potential is defined by the ghost propagator, and the color diagonal ghost propagator is found to be essentially temperature independent. The temperature dependence of the color antisymmetric ghost propagator was not explored. Coulomb gauge is a noncovariant gauge, and the momentum in the time direction is not affected by the gauge fixing. In finite temperature, the momentum in the time direction is interpreted as the Matsubara frequency with appropriate boundary conditions.

The Landau gauge is a covariant gauge, and in the analysis of the quenched and unquenched lattice Landau gauge simulation [5,6], we analyzed zero-temperature $N_f = 2 + 1$ unquenched configuration of the SU(3) MILC collaboration of (1) $20^3 \times 64$ $\beta_{\rm imp} = 6.76$, 6.83, which is denoted as MILC$_c$, since relatively coarse lattice of spacing $a = 0.12$ fm is used, and (2) $28^3 \times 96$ $\beta_{\rm imp} = 7.09$, 7.11, which is denoted as MILC$_f$, since relatively fine lattice of spacing $a = 0.09$ fm is used [7].

We observed that the Kugo-Ojima parameters of MILC$_c$ and MILC$_f$ are consistent with 1 while the quenched configuration of 56^4 lattice remained about 0.8 [8,9]. The Binder cumulant of the color antisymmetric ghost propagator of the zero-temperature quenched SU(2) and unquenched $N_f = 2 + 1$, SU(3) configurations of the MILC collaboration were consistent with those of the $N_c^2 - 1$ dimensional Gaussian distribution, where N_c is the number of colors. The dynamical quark has the effect of quenching randomness of the system [10].

In this paper, we extend the analysis of the color antisymmetric ghost propagator to the quenched SU(3) 56^4 lattices of $\beta = 6.4$ [6] and 6.45 [9] and the finite temperature $N_f = 2$ unquenched SU(3) $24^3 \times 12$ configurations of $\beta = 5.65, 5.725, 5.85$, produced by the MILC collaboration [11]. We denote the finite temperature configurations as MILC$_{ft}$. The ghost propagator contributes in the off-shell quark gluon vertex via Ward-Slavnov-Taylor identity [12], and so we expect the screening masses of the gluons produced by the quark loops and ghost loops would be affected by the ghost propagator. We study the magnetic and the electric screening mass of the gluon of the MILC finite temperature configurations.

In the analysis of [11], the three configurations correspond to the temperature $T = 143$, 172.5, and 185 MeV$_\rho$, respectively, where subscript ρ means that the scale is fixed

*furui@umb.teikyo-u.ac.jp; http://albert.umb.teikyo-u.ac.jp/furui_lab/furuipbs.htm
†nakajima@is.utsunomiya-u.ac.jp

from the mass of the ρ meson $m_\rho = 770$ MeV. The temperature T_c at which the chiral susceptibility shows a peak, indicating the crossover to the deconfinement, was assigned to be about 140 MeV. Since the standard Wilson plaquette action was used in the production of the gauge configuration, the flavor symmetry was broken, and the ratio of the ρ mass to pion mass is larger than the physical value [13]. Recent simulation with Asqtad action [14] suggests that $T_c \sim 170$ MeV, consistent with the value of that of $N_f = 2$ improved Kogut-Susskind (KS) fermion $T_c \sim 173 \pm 8$ MeV [15]. A systematic comparison of the ρ meson mass for improved staggered actions in quenched approximation is given in [16]. Recently, [17] claims that the transition temperature depends on which physical quantity one measures, and that the T_c defined by the chiral susceptibility is 151(3) MeV and consistent within errors with [11]. They showed that the T_c defined by the strange quark chiral susceptibility and the Polyakov loop are about 175 MeV and consistent with [15].

Since the continuum limit of the mass of the vector meson would not depend on the temperature near T_c [18], it would be natural to assign the bare lattice ρ mass by about 20% heavier and shift the temperature by the same amount. We leave a more accurate assignment of the temperature scale of the MILC$_{fl}$ to a future study, and since the disconnected chiral susceptibility measured by the configurations shows a clear peak at around 140 MeV$_\rho$, we assign the $\beta = 5.65$, 5.725, and 5.85 data, which correspond to $T = 143$, 172.5, and 185 MeV$_\rho$, by $T/T_c = 1.02$, 1.23, and 1.32, respectively. We compare the quenched and unquenched ghost propagator of zero temperature and finite temperature and investigate the role of quarks on the gluon field and its dependence on the temperature.

The organization of the paper is as follows. In Sec. II, we show the results of the color diagonal ghost propagator of the quenched 56^4 and unquenched finite temperature MILC configurations. The corresponding color antisymmetric ghost propagators are shown in Sec. III. The Kugo-Ojima parameters, the transverse, magnetic, and electric gluon propagator, and the QCD running coupling of the finite temperature unquenched configurations are shown in Secs. IV, V, and VI, respectively. Conclusions and a discussion are given in Sec. VII.

II. THE COLOR DIAGONAL GHOST PROPAGATOR

The ghost propagator is defined by the Fourier transform (FT) of the expectation value of the inverse Faddeev-Popov operator $\mathcal{M} = -\partial_\mu D_\mu$, where D_μ is the covariant derivative, as

$$FT[D_G^{ab}(x,y)] = FT\langle \mathrm{tr}(\Lambda^{a\dagger}\{(\mathcal{M}[U])^{-1}\}_{xy}\Lambda^b)\rangle = \delta^{ab} D_G(q^2), \quad (1)$$

where U is the link variable obtained by the Landau gauge fixing. In all the simulation in this work we adopt the log$U$ definition of the gauge field, and the SU(3) color matrix Λ is normalized as $\mathrm{tr}\Lambda^a\Lambda^b = \delta^{ab}$. The number of samples is about 10 each in the 56^4 lattices and about 100 each in the $24^3 \times 12$ lattices.

In the usual Monte Carlo simulation, it is necessary to make an average over many samples, but the color diagonal ghost propagator and the color antisymmetric ghost propagator of unquenched configurations are almost independent of samples. Since we adopt the cylinder cut, i.e., select the momentum along the diagonal direction in momentum space, and take into account translation invariance and rotational symmetry of the lattice, the error bar of the ghost propagator of one sample is already not so large, and an order of 10 samples is enough to get the expectation values, although one should be cautious to the appearance of exceptional samples [6].

The color diagonal ghost propagator is defined as

$$D_G(q) = \frac{1}{N_c^2 - 1}\frac{1}{V} \times \mathrm{tr}\langle \delta^{ab}(\langle \Lambda^a \cos qx | f_c^b(x)\rangle + \langle \Lambda^a \sin qx | f_s^b(x)\rangle)\rangle = G(q^2)/q^2.$$

Here $f_c^b(x)$ and $f_s^b(x)$ are the solution of $\mathcal{M} f^b(x) = \rho^b(x)$ with $\rho^b(x) = \frac{1}{\sqrt{V}}\Lambda^b \cos qx$ and $\frac{1}{\sqrt{V}}\Lambda^b \sin qx$, respectively.

A. Quenched SU(3) 56^4 lattice

The color diagonal ghost propagators of 56^4 quenched SU(3) are shown in [6], but we show the data for a comparison with the color antisymmetric ghost propagator in the next subsection. Figure 1 is the ghost dressing function of the 56^4 $\beta = 6.45$ configurations produced by the Monte Carlo simulation and subsequently Landau gauge fixed.

The scale of the $\beta = 6.4$ and 6.45 configurations are fixed as in Table I, using the formula in [19]. The ghost

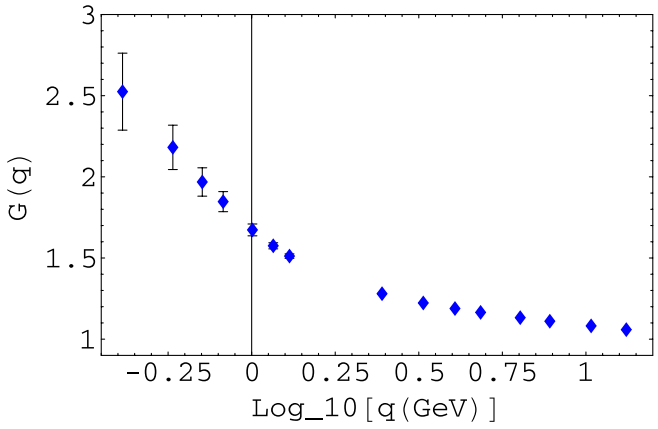

FIG. 1 (color online). The ghost dressing function of quenched 56^4 configurations of $\beta = 6.45$ as the function of $\log_{10}[q(\mathrm{GeV})]$.

TABLE I. The $\beta = 2N_c/g_0^2$ ($\beta_{\rm imp} = 5/3 \times \beta$ for MILC$_f$ and MILC$_c$), the inverse lattice spacing $1/a$, lattice size, and lattice length (fm) of configurations investigated in this paper. Subscripts c and f of MILC correspond to coarse lattice ($a = 0.12$ fm) and fine lattice ($a = 0.09$ fm). The MILC$_{ft}$ corresponds to the $N_f = 2$ finite temperature configurations, and we assign $\beta = 5.65$, 5.725, and 5.85 data to $T/T_c = 1.02$, 1.23, and 1.32, respectively.

	$\beta_{\rm imp}/\beta$	am_{ud}/am_s	N_f	$1/a$ (GeV)	L_s	L_t	aL_s (fm)
quench	6.4		0	3.66	56	56	2.96
	6.45		0	3.87	56	56	2.94
MILC$_c$	6.83	0.040/0.050	2 + 1	1.64	20	64	2.41
	6.76	0.007/0.050	2 + 1	1.64	20	64	2.41
MILC$_f$	7.11	0.0124/0.031	2 + 1	2.19	28	96	2.52
	7.09	0.0062/0.031	2 + 1	2.19	28	96	2.52
MILC$_{ft}$	5.65	0.008	2	1.716	24	12	2.76
	5.725	0.008	2	1.914	24	12	2.47
	5.85	0.008	2	2.244	24	12	2.11

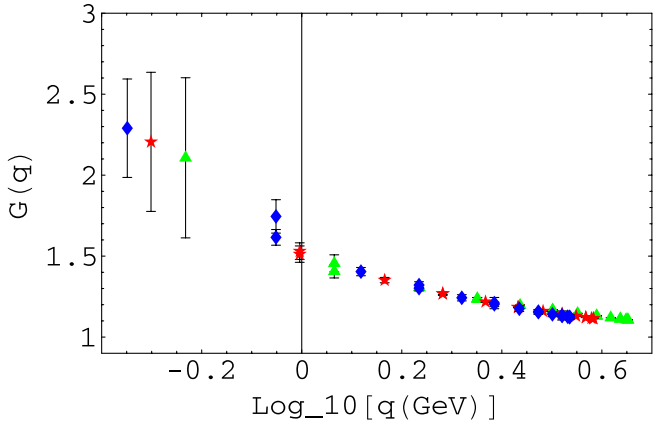

FIG. 2 (color online). The ghost dressing function of MILC$_{ft}$ configurations of $T/T_c = 1.02$ (diamonds), $T/T_c = 1.23$ (stars), and $T/T_c = 1.32$ (triangles) as the function of $\log_{10}[q(\text{GeV})]$.

propagator is infrared divergent, but its singularity is weaker than q^{-4}.

B. MILC finite temperature $24^3 \times 12$ lattice

The color diagonal ghost dressing function of MILC finite temperature configurations are shown in Fig. 2. We observe that the three data of different temperatures scale as shown in the figure when each lattice spacing a is chosen as in Ref. [11].

III. THE COLOR ANTISYMMETRIC GHOST PROPAGATOR

The color antisymmetric ghost propagator is defined as

$$\phi^c(q) = \frac{1}{\mathcal{N}}\frac{1}{V} \times \text{tr}\langle f^{abc}(\langle \Lambda^a \cos qx | f_s^b(x)\rangle - \langle \Lambda^a \sin qx | f_c^b(x)\rangle)\rangle,$$

where the outermost bracket means the ensemble average.

In a theory based on the Curci-Ferrari gauge and in its extension to the Landau gauge, a parametrization of the color antisymmetric ghost propagator with use of the ghost condensate parameter υ was proposed [20].

A simulation in the SU(2) lattice Landau gauge using a parametrization

$$\frac{1}{N_c^2 - 1}\sum_a |\phi^a(q)| = \frac{r/L^2 + \upsilon}{q^4 + \upsilon^2} \tag{2}$$

is performed in [21]. In [20] the ghost propagator in the condensed vacuum in SU(2) is expressed as

$$\langle \bar{c}^a c^b \rangle_q = -i\frac{q^2\delta^{ab} - \upsilon\epsilon^{ab}}{q^4 + \upsilon^2}. \tag{3}$$

The term r/L^2 in Eq. (2) is a term introduced to incorporate the finite lattice size effect. We applied the method to zero-temperature unquenched SU(3) configurations of MILC$_c$ and MILC$_f$ [9,10]. In Ref. [21], the finite size effect expressed by r/L^2 was extracted through the fitting of the lattice data of the color antisymmetric ghost propagator in the high-momentum region, where the perturbative QCD (pQCD) is a good approximation, as

$$\frac{1}{N_c^2 - 1}\sum_a \frac{L^2}{\cos(\pi\bar{q}/L)}|\phi^a(q)| = \frac{r}{q^z}, \tag{4}$$

where the denominator in $\frac{|\phi^a(q)|}{\cos(\pi\bar{q}/L)}$ is the factor that appears in the vertex function of the lattice perturbation theory and $\bar{q}$ takes integer values $0, 1, \cdots L/2$. In the present work, since the high-momentum data points where the enhancement due to $1/\cos$ factor is significant are few, i.e., the enhancement of the highest momentum point of unquenched configuration of MILC$_{ft}$ is 0.64, that of the next to highest momentum point is 0.35 and the rest are less than 0.2 in the $\log_{10}$ scale, we fix the parameter r and υ by the fit of $|\phi^a(q)|$ using Eq. (2) including the whole momentum region except the highest momentum point.

This treatment of the finite size effect on the lattice data is not without ambiguity, but our aim is to search qualitative differences as the temperature or the masses of quarks are changed.

Another quantity that characterizes the system is the Binder cumulant of the color antisymmetric ghost propagator defined as

$$U(q) = 1 - \frac{\langle \vec{\phi}(q)^4 \rangle}{3\langle \vec{\phi}(q)^2 \rangle^2}.$$

A simulation of SU(2) lattice Landau gauge obtained $U \sim 0.44$, almost independent of the momentum. This value is compatible with that of the three-dimensional Gaussian distribution [10] and the analysis of SU(3) MILC$_c$ and MILC$_f$ showed that U is compatible with that of eight-dimensional Gaussian distribution. We extend

these analyses to large quenched lattices and the finite temperature configurations.

A. Quenched SU(3) 56^4 lattice

The absolute value of the color antisymmetric ghost propagator of quenched 56^4 lattice in the infrared region is about 3 orders of magnitude smaller than that of the color diagonal ghost propagator and the values are sample dependent. Results of $\beta = 6.45$, 56^4 10 samples are shown in Fig. 3.

Because of this sample dependence, quite different from the case of unquenched $20^3 \times 64$ lattices [10] and $28^3 \times 96$ [9], the Binder cumulant of the color antisymmetric ghost propagator of quenched configurations is noisy due to large $\langle \vec{\phi}(q)^4 \rangle$ as compared to $\langle \vec{\phi}(q)^2 \rangle^2$. The randomness of the color antisymmetric ghost propagator of quenched configurations is large, and the Binder cumulant becomes unstable.

B. MILC zero-temperature $28^3 \times 96$ lattice

The color antisymmetric ghost propagator of MILC$_f$ is shown in Fig. 4. The fitting parameters are given in [9].

The expectation value of v is small, but the condition that the fitted curve passes the lowest momentum point of Fig. 4 within the error bar gives $v = 0.026(6)$ GeV^2. It suggests that the presence of the BRST (Becchi, Rouet, Stora, and Tyutin) partner of A^2 condensate at zero temperature.

The Binder cumulant of the zero-temperature $N_f = 2 + 1$ MILC$_c$ lattice is reported in [10] and that of MILC$_f$ is reported in [9]. We observed that the mass function of $m_0 = 27.2$ MeV quark propagator of $\beta_{\rm imp} = 7.09$ with bare mass combination $m_0 = 27.2$ MeV/68 MeV shows an anomalous behavior in the $q < 1$ GeV region, and that in the same region Binder cumulant $U(q)$ shows an anomalous behavior, although the mass function of $m_0 = 68$ MeV does not show the anomaly. The non-QCD-like behavior of staggered quarks calculated with large lattice spacing a and small bare mass m_0 is reported in [22]. Since no anomaly was observed in $\beta = 7.09$ $m_0 = 13.6$ MeV/68 MeV [9,10], effects of the relative size of the s-quark mass vs ud-quark mass and the number of N_f are suggested.

Thus we extend the analysis to MILC configuration of $N_f = 3$, $\beta_{\rm imp} = 7.18$, $28^3 \times 96$ lattice with the bare quark mass $m_0 = 0.031$ and that of $N_f = 2$, $\beta_{\rm imp} = 7.20$, $20^3 \times 64$ lattice with the bare quark mass $m_0 = 0.02$ [23]. A result of the Binder cumulants of the $N_f = 3$ and the $N_f = 2$ (50 samples) are 0.66(1), i.e., $\langle \vec{\phi}(q)^4 \rangle$ is close to $\langle \vec{\phi}(q)^2 \rangle^2$. When the bare masses of the quarks are the same, the system possesses the self-averaging property [24], and when they are different as in $N_f = 2 + 1$, the system lacks this property. The parameter v fitted from $N_f = 2$ (50 samples) is found to be consistent with 0.

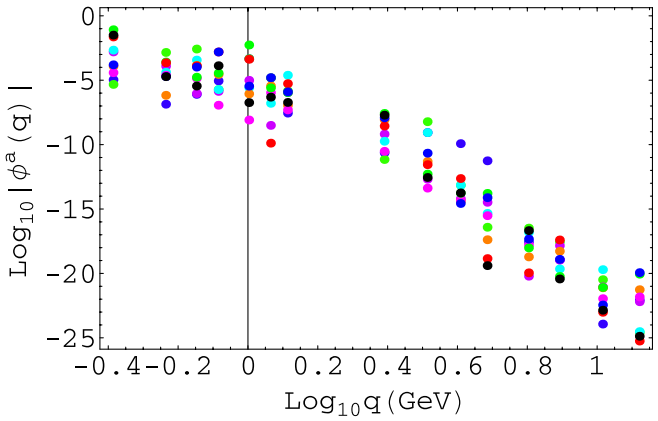

FIG. 3 (color online). $\log_{10}|\vec{\phi}(q)|$ as the function of $\log_{10} q$(GeV) of quenched $\beta = 6.45$, 56^4 lattice.

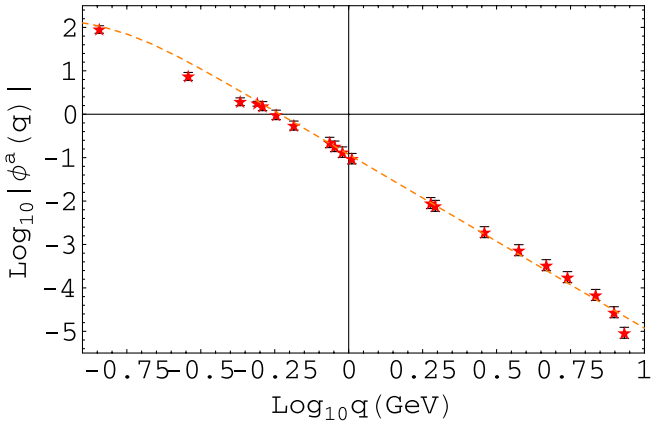

FIG. 4 (color online). $\log_{10}|\vec{\phi}(q)|$ as the function of $\log_{10} q$(GeV) of MILC$_f$ and the fit using $r = 134$ and $v = 0.026$ GeV^2.

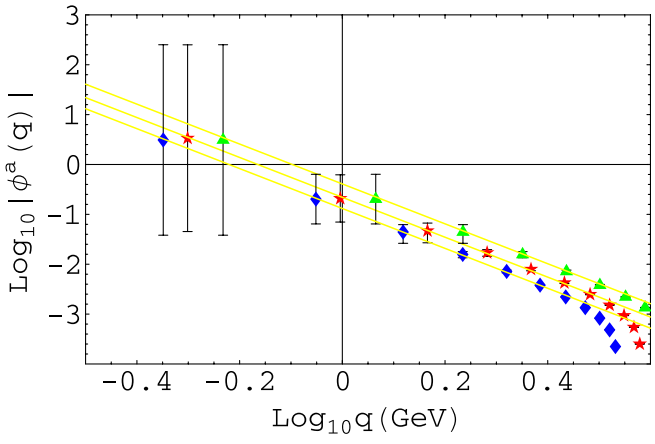

FIG. 5 (color online). $\log_{10}|\vec{\phi}(q)|$ as the function of $\log_{10} q$(GeV) of MILC$_{ft}$ of $T/T_c = 1.02$ (diamonds), $T/T_c = 1.23$ (stars), and $T/T_c = 1.32$ (triangles).

TABLE II. The fitted parameters r, z, and v of the color antisymmetric ghost propagator $|\phi(q)|$ of MILC$_c$, MILC$_f$, and MILC finite temperature. Two values of U of MILC$_f$ correspond to the average below $q = 1$ GeV and the average above 1 GeV, respectively.

$\beta_{\rm imp}/\beta$	m_0 (MeV)	r	z	v	U
6.76	11.5/82.2	37.5	3.90	0.02(1)	0.53(5)
6.83	65.7/82.2	38.7	3.85	0.01(1)	0.57(4)
7.09	13.6/68.0	134	3.83	0.026(6)	0.57(4)/0.56(1)
7.11	27.2/68.0	112	3.81	0.028(8)	0.58(2)/0.52(1)
5.65	12.3	54.4	4.01	0.0	0.580(13)
5.725	12.8	88.3	3.95	0.0	0.571(4)
5.85	15.0	165.9	3.93	0.0	0.558(2)

C. MILC finite temperature $24^3 \times 12$ lattice

The fluctuation of the color antisymmetric ghost propagator around the expectation value 0 was almost Gaussian in the case of zero-temperature unquenched configurations [9,10]. The logarithm of the absolute value of the color antisymmetric ghost propagator of finite temperature unquenched configurations as a function of the logarithm of the momentum is shown in Fig. 5. In contrast to the color diagonal ghost propagator, the absolute value of the color antisymmetric ghost propagator depends on the temperature. The temperature dependence of the scale of ϕ defined by r of Eq. (4) can be expressed as roughly $r \sim 5.49a^{-4.23}$, where a is the lattice spacing at each temperature in the unit of GeV.

The fitting parameters of the color antisymmetric ghost propagator are given in Table II. The condensate parameter v of finite temperature is difficult to assign since the lattice spacing is relatively large and it is difficult to detect the infrared bending behavior in the color antisymmetric ghost propagator, but they are consistent with 0.

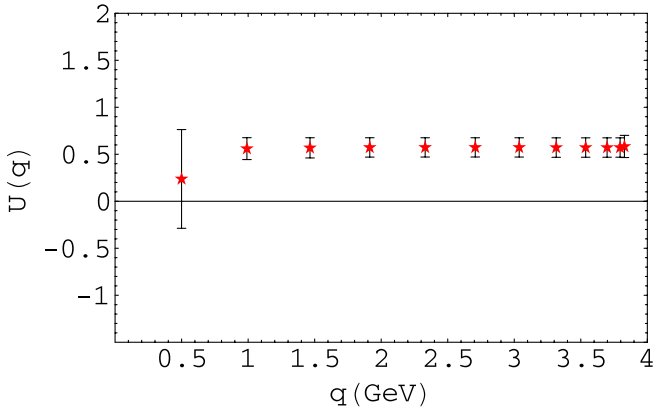

FIG. 6 (color online). The Binder cumulant of the color antisymmetric ghost propagator of MILC $N_f = 2$ configurations of $T/T_c = 1.23$ (stars).

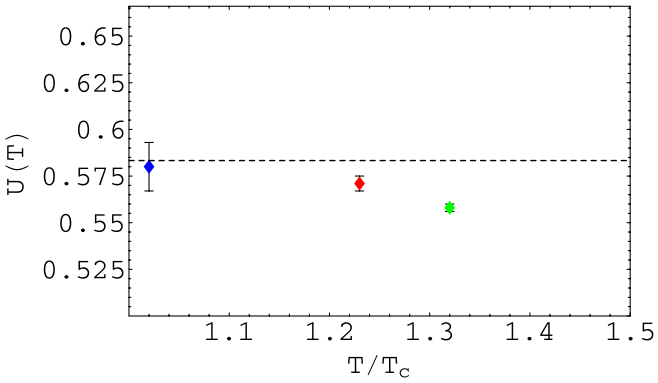

FIG. 7 (color online). Averages over momenta excluding the lowest momentum point of the Binder cumulants of MILC finite temperature configurations. $T/T_c = 1.02$ (diamonds), $T/T_c = 1.23$ (stars), and $T/T_c = 1.32$ (triangles).

The Binder cumulant of ϕ is almost independent of the momentum except the lowest momentum point. We show a typical example of $T/T_c = 1.23$ in Fig. 6.

The temperature dependence of the average of $U(q)$ excluding the lowest momentum point is shown in Fig. 7. The average $U(T)$ decreases monotonically as a function of T from that of the Gaussian distribution (dashed line) at high temperature.

IV. THE KUGO-OJIMA COLOR CONFINEMENT PARAMETER

The Kugo-Ojima parameter is defined by the two-point function of the covariant derivative of the ghost and the commutator of the antighost and gauge field

$$\left(\delta_{\mu\nu} - \frac{q_\mu q_\nu}{q^2}\right) u^{ab}(q^2) = \frac{1}{V}\sum_{x,y} e^{-iq(x-y)} \times \left\langle \mathrm{tr}\left(\Lambda^{a\dagger} D_\mu \frac{1}{-\partial D}[A_\nu, \Lambda^b]\right)_{xy}\right\rangle. \tag{5}$$

Kugo and Ojima [1] showed that $u(0) = -1$ is a condition of the color confinement. Zwanziger [3] defined the horizon function h that is related to the Kugo-Ojima parameter $c = -u(0)$ as follows:.

$$\sum_{x,y} e^{-iq(x-y)} \left\langle \mathrm{tr}\left(\Lambda^{a\dagger} D_\mu \frac{1}{-\partial D}(-D_\nu)\Lambda^b\right)_{xy}\right\rangle = G_{\mu\nu}(q)\delta^{ab} = \left(\frac{e}{d}\right)\frac{q_\mu q_\nu}{q^2}\delta^{ab} - \left(\delta_{\mu\nu} - \frac{q_\mu q_\nu}{q^2}\right)u^{ab},$$

where, with use of the covariant derivative $D_\mu(U)$,

$$D_\mu(U_{x,\mu})\phi = S(U_{x,\mu})\partial_\mu\phi + [A_{x,\mu}, \bar{\phi}],$$

$\partial_\mu\phi = \phi(x+\mu) - \phi(x)$, $\bar{\phi} = \frac{\phi(x+\mu)+\phi(x)}{2}$, and $S(U_{x\mu}) = \frac{adjA_{x,\mu}/2}{\tanh(adjA_{x,\mu}/2)}$.

Using the definition

$$e = \left\langle \sum_{x,\mu} \mathrm{tr}(\Lambda^{a\dagger} S(U_{x,\mu})\Lambda^a) \right\rangle \Big/ \{(N_c^2 - 1)V\},$$

the horizon condition reads $\lim_{q\to 0} G_{\mu\mu}(q) - e = 0$, and the left-hand side of the condition is $\frac{e}{d} + (d-1)c - e = (d-1)h$ where $c - \frac{e}{d}$, where $d = 4$ is the dimension of the system. It follows that $h = 0$ is the horizon condition, and thus the horizon condition coincides with Kugo-Ojima criterion provided the covariant derivative approaches the naive continuum limit, i.e., $e/d = 1$.

The Kugo-Ojima parameter is defined by a scalar function at vanishing momentum in the continuum theory, but in the lattice simulation, we measured the magnitude of the right-hand side of Eq. (5) with $\mu = \nu$ polarizations of A_ν and D_μ, and then observed in the case of asymmetric lattices there is a strong positive correlation between the magnitude and the lattice size of the axis whose directions are perpendicular to the polarization. These general features are manifested in the data of MILC$_f$ and MILC$_c$ whose time (4th) axis is longer than the spatial axes, and in the data of MILC$_{ft}$ whose time axis is shorter than the spatial axes.

A. Quenched SU(3) 56^4 lattice

The Kugo-Ojima confinement parameter of quenched configuration saturates at about 80% of the expected value $c = 1$. There appear exceptional samples with an average consistent with $c = 1$ within errors. The polarization dependence of the Kugo-Ojima parameter of $\beta = 6.45$ samples shown in Fig. 8 is due to the lack of rotational invariance of our system.

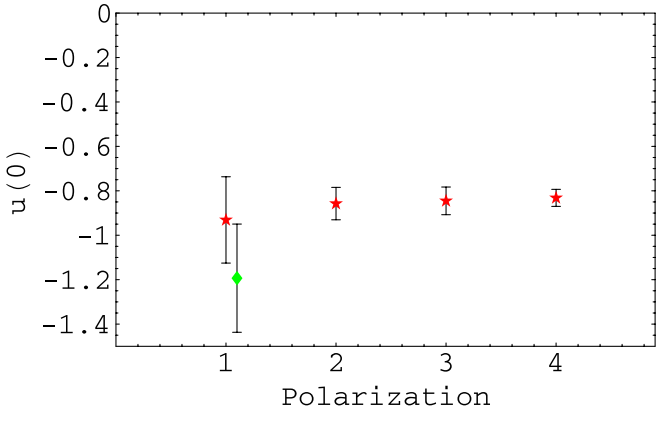

FIG. 8 (color online). Kugo-Ojima parameter $u(0)$ of quenched 56^4 configurations of $\beta = 6.45$ (stars). The data of an exceptional sample is indicated by the diamond. Polarizations 1, 2, 3, 4 correspond to x, y, z, and t.

TABLE III. The Kugo-Ojima parameter of the quenched 56^4 lattice and that of the unquenched KS fermion (MILC$_c$, MILC$_f$, MILC$_{ft}$). c_x is the polarization along the spatial directions; c_t is that along the time direction; c is the weighted average of c_x and c_t, i.e., $(3c_x + c_t)/4$; e/d is the trace divided by the dimension; and h is the horizon function deviation.

	$\beta_{\mathrm{imp}}/\beta$	c_x	c_t	c	e/d	h
quench	6.4			0.827(27)	0.954(1)	−0.12
	6.45			0.814(89)	0.954(1)	−0.14
MILC$_c$	6.76	1.04(11)	0.74(3)	0.97(16)	0.9325(1)	0.03(16)
	6.83	0.99(14)	0.75(3)	0.93(16)	0.9339(1)	−0.00(16)
MILC$_f$	7.09	1.06(13)	0.76(3)	0.99(17)	0.9409(1)	0.04(17)
	7.11	1.05(13)	0.76(3)	0.98(17)	0.9412(1)	0.04(17)
MILC$_{ft}$	5.65	0.72(13)	1.04(23)	0.80(21)	0.9400(7)	−0.14(21)
	5.725	0.68(15)	0.77(16)	0.70(15)	0.9430(2)	−0.24(15)
	5.85	0.63(19)	0.60(12)	0.62(17)	0.9465(2)	−0.33(17)

B. MILC finite temperature $N_f = 2$, $24^3 \times 12$ lattice

Shown in Table III are the Kugo-Ojima parameters and the horizon function deviation of quenched 56^4 configurations, zero-temperature unquenched MILC$_c$ and MILC$_f$ configurations, and unquenched finite temperature MILC$_{ft}$ configurations.

The Kugo-Ojima parameters of unquenched zero-temperature configurations are consistent with the theory [8–10], and those of unquenched finite temperature configurations show temperature dependence.

Figure 9 shows the dependence on the polarization of the Kugo-Ojima parameter. The polarization dependence of the parameter c is a result of an integration over the axes perpendicular to the polarization. It becomes large when there is a long axis perpendicular to the polarization. Figure 10 shows the temperature and the polarization dependence of the Kugo-Ojima parameter.

The quenched configurations and high-temperature configurations show larger deviation from $u(0) = -1$, which

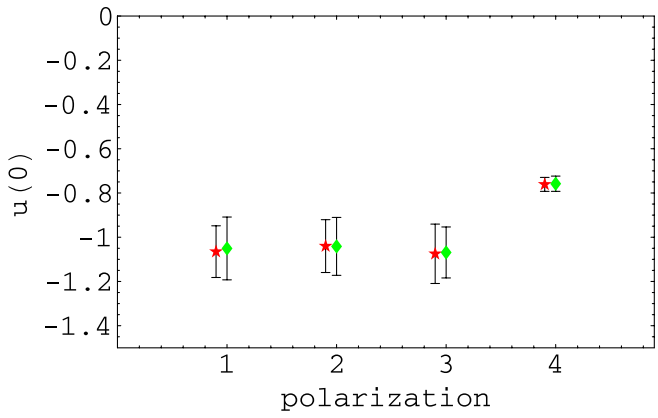

FIG. 9 (color online). Kugo-Ojima parameter $u(0)$ of MILC$_f$ $N_f = 2 + 1$ KS fermion unquenched configurations of $\beta_{\mathrm{imp}} = 7.11$ (diamonds), $\beta_{\mathrm{imp}} = 7.09$ (stars).

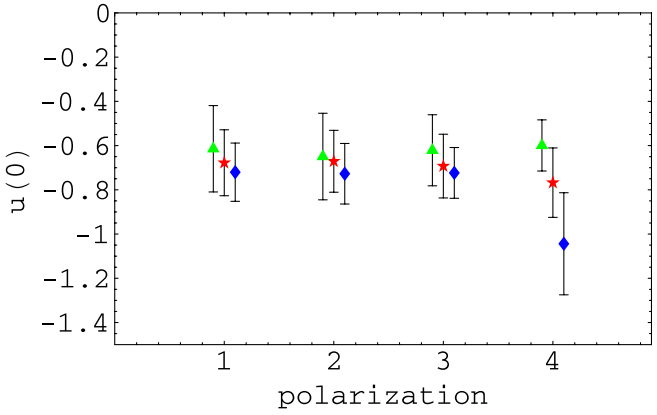

FIG. 10 (color online). Kugo-Ojima parameter $u(0)$ of MILC$_{ft}$ configurations of $T/T_c = 1.02$ (diamonds), $T/T_c = 1.23$ (stars), and $T/T_c = 1.32$ (triangles).

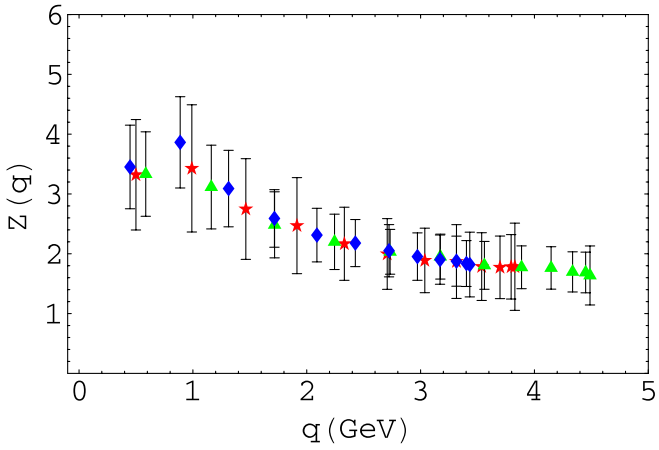

FIG. 11 (color online). The transverse gluon dressing function $Z(q)$ of MILC$_{ft}$ $N_f = 2$ KS fermion unquenched configuration of $T/T_c = 1.02$ (diamonds), $T/T_c = 1.23$ (stars), and $T/T_c = 1.32$ (triangles).

would be due to higher randomness of these systems. The origin of the randomness in the latter would be the thermal fluctuation and that of the former would be the lack of fermions that quench randomness of the system.

V. THE FINITE TEMPERATURE GLUON PROPAGATOR

The fluctuation of the gluon propagators of lattice Landau gauge is larger than that of the ghost propagator. We measure the gluon propagators of the three temperatures of MILC$_{ft}$ by using about 100 samples each and choosing the momenta along the three-dimensional (3D) coordinate axes and along the diagonal in the 3D space. The dependence on the choice of the direction is not significant except a slight suppression of the $\bar{q} = (1, 1, 1, 0)$, as compared to that with the same magnitude but along the coordinate axes. We fix the normalization of the gluon propagator such that the running coupling defined by the product of the gluon dressing function and the ghost dressing function squared as defined in Sec. VI in the high-momentum region agrees with the pQCD result and that the rescaling factor for the ghost dressing function and the gluon dressing function are the same. The renormalization factors defined by the highest momentum point along the coordinate axes of the three temperatures are 0.48(1).

In Fig. 11 the transverse gluon dressing functions of the three temperatures taken at momenta along the diagonal direction in the 3D momentum space after the rescaling are shown. The asymptotic value is about 2, since we normalized $\mathrm{Tr}\Lambda^a\Lambda^b = \delta^{ab}$. Larger infrared enhancement of the transverse gluon dressing function for low temperature agrees with a recent result of quenched SU(2) finite temperature simulation [25].

The transverse gluon propagator at the zero momentum is finite as shown in Fig. 12. The value of $D_A(0)$ of MILC$_f$, $\beta = 7.09$, $28^3 \times 96$ is about 15 GeV^{-2} [8]. The $D_A(0)$ decreases monotonically as T decreases to 0. Whether it vanishes or remains finite is an important problem for fixing the nature of the infrared fixed point of the running coupling. There is an argument that the infrared nonvanishing of the Landau gauge gluon propagator is a finite size effect. Our lattice volume of low-temperature data is larger than the high-temperature data, but the running coupling which is calculated by the gluon propagator and shown in Sec. VI excludes large temperature dependence in the finite size effects. A correction of the global scaling factor is, however, not excluded.

We observe that the fluctuation of the gluon propagator at the zero momentum increases as the temperature increases.

The one-loop off-shell contribution to the quark-gluon vertex is related to the quark-quark-ghost-ghost amplitude via Ward-Slavnov-Taylor identity [12]. The screening

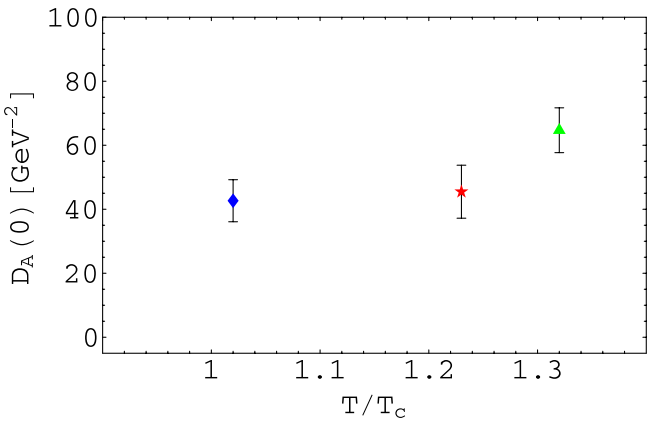

FIG. 12 (color online). The transverse gluon propagator of MILC$_{ft}$ $N_f = 2$ KS fermion unquenched configuration of $T/T_c = 1.02$ (diamonds), $T/T_c = 1.23$ (stars), and $T/T_c = 1.32$ (triangles) at $q = 0$ in the unit of GeV^{-2}.

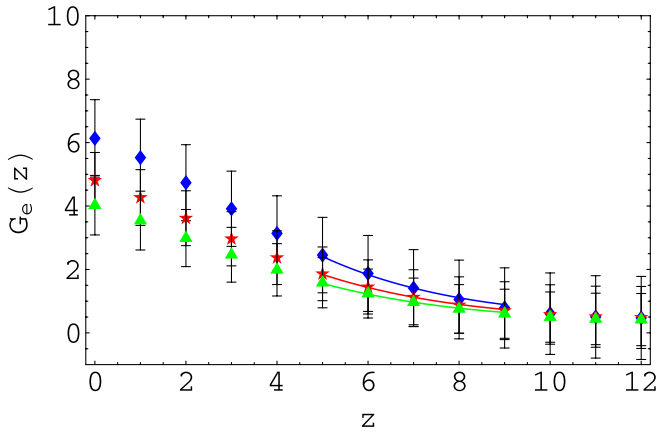

FIG. 13 (color online). Electric gluon propagator of MILC$_{ft}$ $N_f = 2$ KS fermion unquenched configuration of $T/T_c = 1.02$ (diamonds), $T/T_c = 1.23$ (stars), and $T/T_c = 1.32$ (triangles).

mass of the gluon would be affected by the ghost propagator. The correlation function of the gauge fields in the position space is defined as [26]

$$D_{A\mu}(z) = \langle A_\mu(z) A_\mu(0) \rangle,$$

where $A_\mu(z) = \sum_{x_0,x_1,x_2} A_\mu(x_0, \vec{x})$.

The screening mass of the gluon is produced by the quark-, gluon-, and ghost-loops. The electric screening mass m_e is defined by

$$G_e(z) = D_{A0}(z) \sim \exp[-m_e z/N_t T].$$

The magnetic screening mass m_m is defined by

$$G_m(z) = (D_{A1}(z) + D_{A2}(z))/2 \sim \exp[-m_m z/N_t T].$$

We fit the propagator $G_e(z)$ and $G_m(z)$ by

$$D_A(z) = A \cosh[(m/N_t T)(z - N_x/2)].$$

The mass depends on the region of z used to fit the data and Karsch *et al.* proposed to fit data of z near $N_x/4$ [27]. We fit

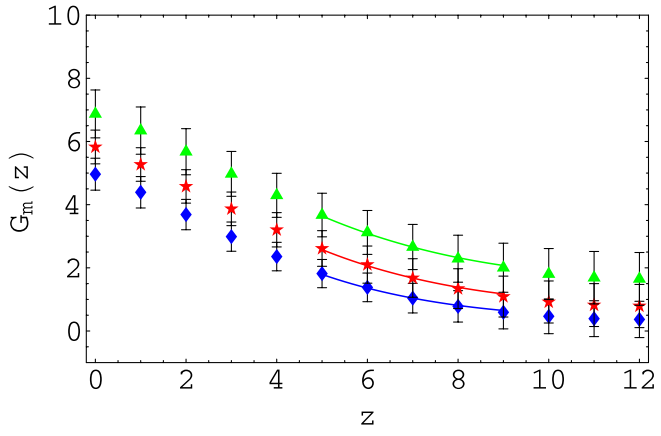

FIG. 14 (color online). Magnetic gluon propagator of MILC$_{ft}$ $N_f = 2$ KS fermion unquenched configurations of $T/T_c = 1.02$ (diamonds), $T/T_c = 1.23$ (stars), and $T/T_c = 1.32$ (triangles).

TABLE IV. The electric and the magnetic screening mass of MILC$_{ft}$.

β	T/T_c	m_e/T	m_m/T
5.65	1.02	3.42(27)	3.48(48)
5.725	1.23	3.22(40)	2.90(20)
5.85	1.32	3.14(33)	2.31(22)

the data from $z = 5$ to 9. When we fit the data from $z = 0$ to $z = 6$, the masses become smaller by about 30–40%. Since deviations from the cosh functional form become larger in this region, we adopt the fit from $z = 5$ to 9. The fitted data of MILC$_{ft}$ electric gluon propagator $G_e(z)$ and the magnetic gluon propagator $G_m(z)$ are shown in Fig. 13 and Fig. 14, respectively.

In high temperature, pQCD suggests that

$$\frac{m_e}{T} \propto g(T), \qquad \frac{m_m}{T} \propto g^2(T),$$

where $g^2(T)/4\pi$ is the running coupling at temperature T and 0 momentum. Our electric screening mass and the magnetic screening mass are close to those of quenched SU(2) $m_e/T = 2.484(52)$ measured by [26]. The magnetic screening mass in the case of SU(2) using the data in the region of $T > 2T_c$ was $m_m/T = 0.466(25)g^2(T)$ in the two-loop pQCD calculation with $\Lambda_m = 0.262(18)T_c$. In the case of quenched SU(3), [28] obtained, using the data in the region of $T > 1.5T_c$, $m_e/T = 1.69(4)g(T)$ and $m_m/T = 0.549(16)g^2(T)$. Since the electric and the magnetic gluon propagator of [28] are normalized to 1 at $z = 0$ and the critical temperature of the quenched configuration $T_c \sim 269 \pm 1$ MeV [15] is much higher than that of the unquenched configuration, we cannot compare quantitatively their data with ours, but their data of $T/T_c = 1.32$ are consistent with ours within errors. We do not observe suppression of m_e/T near T_c. Whether the discrepancy is due to the presence of dynamical quarks is left for future study. Discrepancy of about factor 6 in the m_m/T of SU(3) near T_c from the extrapolation of the pQCD results in $T > 1.5T_c$ region implies breakdown of the perturbation series near T_c.

VI. THE FINITE TEMPERATURE QCD RUNNING COUPLING

In [29] the calculation of the running coupling in the Dyson-Schwinger equation (DSE) at zero temperature [30] was extended to below T_c and the running coupling for $q_0 = 2\pi n T$ is written as

$$\alpha(n, \boldsymbol{q}^2, T) = \alpha(\mu^2) G^2(n, \boldsymbol{q}^2, \mu^2, T) Z(n, \boldsymbol{q}^2, \mu^2, T), \quad (6)$$

where $G(n, \boldsymbol{q}^2, \mu^2, T)$ is the ghost dressing function and $Z(n, \boldsymbol{q}^2, \mu^2, T)$ is the gluon dressing function. Applying this method to $T \sim T_c$, we measure the QCD running coupling in the asymmetric momentum subtraction ($\widetilde{MOM}$) scheme as the product of the gluon dressing

function and the ghost dressing function squared, as a function of the momentum $\boldsymbol{q}$ along the spatial axes. We set n equal to 0 in the analysis. We normalize the magnitude to the result of four-loop pQCD [8,31–33] at the highest momentum point of $\beta = 5.725$. A DSE result of zero-temperature quenched configuration with the infrared exponent of the ghost propagator $\kappa = 0.5$ [34]. In [6] we compared the running coupling in the quenched lattice simulation with the parametrization suggested by the DSE analysis as[1]

$$\alpha_s(q^2) = \frac{1}{c_0 + (q^2/\Lambda_{\rm QCD}^2)^2}\Bigg[c_0\alpha_0 + \frac{4\pi}{\beta_0} \times \left(\frac{1}{\log(q^2/\Lambda_{\rm QCD}^2)} - \frac{1}{(q^2/\Lambda_{\rm QCD}^2) - 1}\right)\left(\frac{q^2}{\Lambda_{\rm QCD}^2}\right)^2\Bigg], \tag{7}$$

where $\beta_0 = 11 - \frac{2}{3}N_f$.

The parameters adopted in the fit were $\Lambda_{\rm QCD} = 330$ MeV, $c_0 = 30$. The N_f dependence of the running coupling is not so large, and to make comparison with the quenched data the dashed line used to fit the quenched data of $N_f = 0$ [6] is shown in Fig. 16.

In the pQCD, an approximate inversion of the four-loop formula yields the running coupling as a function of $t = \log(q^2/\Lambda^2)$ as follows [31,32].

$$\alpha_{s,\rm pert}(q^2) = \frac{4\pi}{\beta_0 t} - \frac{8\pi\tilde{\beta}_1}{\beta_0}\frac{\log(t)}{(\beta_0 t)^2} + \frac{1}{(\beta_0 t)^3}\Bigg(\frac{2\pi\tilde{\beta}_2}{\beta_0} + \frac{16\pi\tilde{\tilde{\beta}}_1^2}{\beta_0^2}(\log^2(t) - \log(t) - 1)\Bigg) + \frac{1}{(\beta_0 t)^4} \times \Bigg[\frac{2\pi\tilde{\beta}_3}{\beta_0} + \frac{16\pi\tilde{\beta}_1^3}{\beta_0^3}\Bigg(-2\log^3(t) + 5\log^2(t) + \left(4 - \frac{3\tilde{\beta}_2\beta_0}{4\tilde{\beta}_1^2}\right)\log(t) - 1\Bigg)\Bigg], \tag{8}$$

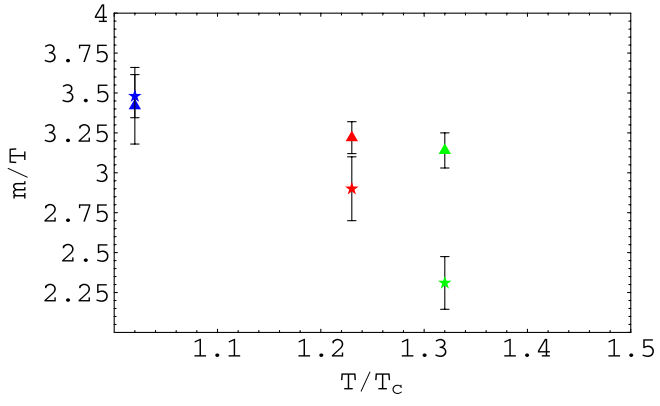

FIG. 15 (color online). The magnetic screening mass m_m/T (stars) and the electric screening mass m_e/T of MILC$_{ft}$ $N_f = 2$ KS fermion unquenched configurations (triangles).

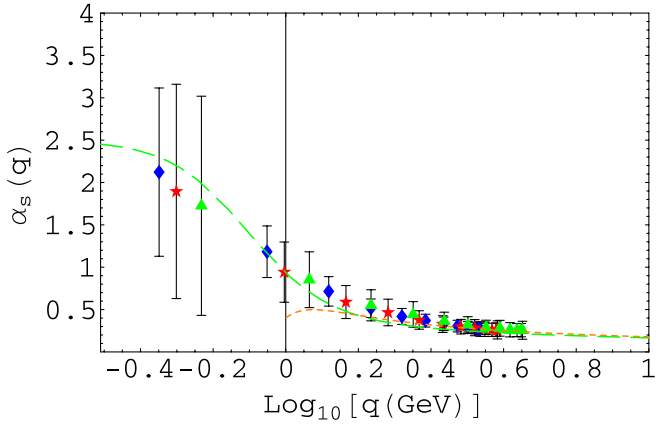

FIG. 16 (color online). The running coupling of the MILC$_{ft}$ of $\beta = 5.65$ (diamonds), 5.725 (stars), and 5.85 (triangles) as the function of $\log_{10}q$(GeV). The dashed line is the DSE result used to fit the quenched zero-temperature lattice data [6] with $\kappa = 0.5$, and the dotted line is the pQCD result with $N_f = 2$ of zero temperature.

where $\tilde{\beta}_1 = (102 - \frac{38}{3}N_f)/2$, and

$$\tilde{\beta}_2 = \left(\frac{2857}{2} - \frac{5033}{18}N_f + \frac{325}{54}N_f^2\right)\Big/4,$$

$$\tilde{\beta}_3 = \Bigg(\frac{149753}{6} + 3564\zeta(3) + \Bigg(-\frac{1078361}{162}N_f - \frac{6508}{27}N_f\zeta(3)\Bigg) + \left(\frac{50065}{162} + \frac{6472}{81}\zeta(3)\right)N_f^2 + \frac{1093}{729}N_f^3\Bigg)\Big/8.$$

Here the scale in the $\widetilde{MOM}$ scheme is defined as [35,36]

$$\Lambda = \Lambda_{\overline{MS}}e^{(70/3-22N_f/9)/22},$$

and $\Lambda_{\overline{MS}}$ is 0.259(22) GeV for $N_f = 2$ and 0.252(10) GeV for $N_f = 0$ were obtained by fitting the data in the continuum window $1.8\ {\rm GeV} < q < 2.3\ {\rm GeV}$ ($0.26 < \log_{10}[q({\rm GeV})] < 0.37$)[31,36].

The pQCD running coupling in the $\widetilde{MOM}$ scheme using $\Lambda_{\overline{MS}} = 0.259$ GeV is shown by the dotted line.

Comparing with the result of $N_f = 2 + 1$ zero temperature [8], the deviation from the pQCD is smaller. Although the presence of ghost condensate at zero temperature is not excluded, there is no sign of finite v and A^2 at finite temperature.

The running couplings of three temperatures near T_c as a function of the momentum $\boldsymbol{q}$ lie roughly on a single curve and there is not strong temperature dependence. The relatively large T dependence of the m_m/T suggests that the

[1]We use $\log(t)$ representing $\ln(t)$. The common logarithm is expressed as $\log_{10}$.

nonperturbative effects on the magnetic screening mass are important.

The running coupling of zero-temperature $N_f = 2$ MILC $20^3 \times 64$ configuration is roughly the same as that of $N_f = 2 + 1$ MILC$_c$ presented in Fig. 15 of [8]. In the $-0.9 < \log_{10}[q(\mathrm{GeV})] < -0.3$ region it decreases monotonically. We think that the suppression of the running coupling at the infrared is due to the singularity of the color antisymmetric ghost dressing function there, which suppresses the color diagonal ghost dressing function, and that the suppression is a kind of an artifact. It may imply a question on the structure of the infrared fixed point and on the extensibility from the perturbative region to the nonperturbative region of the method of defining the running coupling from the product of the color diagonal ghost dressing function squared and the gluon dressing function.

VII. DISCUSSION AND CONCLUSION

We measured the color diagonal and the color antisymmetric ghost propagator of quenched, unquenched zero-temperature and unquenched finite temperature configurations. The quark has the effect of quenching randomness of the ghost propagator and enhancing the transverse and magnetic gluon propagator above T_c. The Binder cumulant of the quenched SU(3) color antisymmetric ghost propagator is noisy, but that of the unquenched SU(3) color antisymmetric ghost propagator is almost constant and independent of the momentum except the lowest momentum point. The color diagonal ghost propagator of finite temperatures above T_c is almost temperature independent, but the scale of the color antisymmetric ghost propagator becomes larger as the temperature becomes higher.

We observed that the Binder cumulants of unquenched SU(3) $N_f = 2 + 1$ configurations at zero temperature are consistent with those of $N_c^2 - 1$ dimensional Gaussian distribution when the strange quark mass is not close to the ud-quark mass, and that $N_f = 2$ configurations at finite temperatures deviate from Gaussian distribution as the temperature rises from T_c, which may be interpreted as the quark effect of quenching randomness is reduced in high temperature. The anomaly of the KS fermion propagator and that of the momentum dependence of the Binder cumulant seem to be correlated. This may indicate that the QCD-like region of the $N_f = 2 + 1$ KS fermion system is more complicated than that of the $N_f = 2$ case given in [22]. The Binder cumulant of unquenched $N_f = 2$ and 3 which are consistent with 0.66 indicates that the ratio of the ud-quark mass and the s-quark mass is an important ingredient.

The parameter υ introduced to investigate the ghost condensate is found to be small, and its value depends on the temperature and the bare mass of the KS fermion.

We observed strong nonperturbative effects in the magnetic screening mass of the gluon near T_c. Since near T_c systematic perturbative QCD calculation is impossible, it is important to formulate the lattice theory. In the quenched finite temperature Landau gauge DSE approach [29,37] the infrared exponent κ and the running coupling in the momentum subtraction scheme were found to be essentially temperature independent below T_c.

ACKNOWLEDGMENTS

We thank F. Karsch for a discussion on the scale assignment of the lattice data and A. Nakamura and T. Saito for the information on the quenched simulation of their group. This work is supported by the High Energy Accelerator Research Organization (KEK) supercomputer project No. 05-128 using Hitachi-SR8000 and the large-scale simulation program No. 5 (FY2006) using SR11000. Numerical calculation of the ghost propagator was carried out by NEC-SX5 at the CMC of Osaka University and by NEC-SX8 at the Yukawa Institute Computer Facility in Kyoto University. H. N. is supported by the MEXT grant in aid of scientific research in priority area No. 13135210.

[1] T. Kugo and I. Ojima, Prog. Theor. Phys. Suppl. **66**, 1 (1979).
[2] V. N. Gribov, Nucl. Phys. **B139**, 1 (1978).
[3] D. Zwanziger, Nucl. Phys. **B364**, 127 (1991); **B412**, 657 (1994).
[4] J. Greensite, S. Olejník, and D. Zwanziger, Phys. Rev. D **69**, 074506 (2004).
[5] S. Furui and H. Nakajima, Phys. Rev. D **69**, 074505 (2004); arXiv: hep-lat/0305010.
[6] S. Furui and H. Nakajima, Phys. Rev. D **70**, 094504 (2004); arXiv: hep-lat/0403021.
[7] C. Bernard *et al.*, Phys. Rev. D **58**, 014503 (1998).
[8] S. Furui and H. Nakajima, Few-Body Syst. **40**, 101 (2006); arXiv:hep-lat/0503029.
[9] S. Furui and H. Nakajima, in *Proceedings of IRQCD, Rio de Janeiro, 2006* [Braz. J. Phys. 37, 186 (2007)]; arXiv:hep-lat/0609024.
[10] S. Furui and H. Nakajima, Phys. Rev. D **73**, 074503 (2006); arXiv:hep-lat/0511045.
[11] C. Bernard *et al.*, Phys. Rev. D **54**, 4585 (1996).
[12] A. I. Davydychev, P. Osland, and L. Saks, Phys. Rev. D **63**, 014022 (2000).
[13] T. Blum, L. Kärkkäinen, D. Toussaint, and S. Gottlieb, Phys. Rev. D **51**, 5153 (1995).
[14] C. Bernard *et al.*, Phys. Rev. D **75**, 094505 (2007); arXiv:hep-lat/0611031.
[15] F. Karsch and E. Laermann, in *Quark-Gluon Plasma III*, edited by R. C. Hwa and X. N. Wang (World Scientific,

New York, 2004); arXiv: hep-lat/0305025.
[16] M. Cheng, N. Christ, C. Jung, F. Karsch, R. Mawhinney, P. Petrecky, and K. Petrov, Phys. Lett. B **643**, 311 (2006); arXiv:hep-lat/0612030 v1.
[17] Y. Aoki, Z. Fodor, S. D. Katz, and K. K. Szabó, Phys. Lett. B **643**, 46 (2006).
[18] F. Karsch, in *Selected Topics in Non Perturbative QCD, "Enrico Fermi School," 1995*, edited by A. Di Giacomo and D. Diakonov (IOS Press, Amsterdam, 1997) pp. 51–71; arXiv: hep-lat/9512029.
[19] S. Necco and R. Sommer, Nucl. Phys. **B622**, 328 (2002); arXiv: hep-lat/0108008.
[20] D. Dudal *et al.*, J. High Energy Phys. 06 (2003) 003.
[21] A. Cucchieri, T. Mendes, and A. Mihara, Phys. Rev. D **72**, 094505 (2005).
[22] A. Hasenfratz and R. Hoffmann, Phys. Rev. D **74**, 014511 (2006).
[23] C. Bernard *et al.*, Phys. Rev. D **64**, 054506 (2001); arXiv:hep-lat/0104002.
[24] D. P. Landau and K. Binder, *A Guide to Monte Carlo Simulations in Statistical Physics* (Cambridge University Press., Cambridge, England, 2005).
[25] A. Cucchieri, A. Maas, and T. Mendes, Phys. Rev. D **75**, 076003 (2007); arXiv:hep-lat/0702022.
[26] U. M. Heller, F. Karsch, and J. Rank, Phys. Lett. B **355**, 511 (1995); arXiv: hep-lat/9505016.
[27] U. M. Heller, F. Karsch, and J. Rank, Phys. Rev. D **57**, 1438 (1998).
[28] A. Nakamura, T. Saito, and S. Sakai, Phys. Rev. D **69**, 014506 (2004).
[29] B. Grüter, R. Alkofer, A. Maas, and J. Wambach, Eur. Phys. J. C **42**, 109 (2005); arXiv:hep-ph/0408282.
[30] L. von Smekal, A. Hauck, and R. Alkofer, Ann. Phys. (N.Y.) **267**, 1 (1998).
[31] Ph. Boucaud *et al.*, J. High Energy Phys. 01 (2002) 046; arXiv:hep-lat/0107278.
[32] K. G. Chetyrkin and A. Rétay, arXiv:hep-ph/0007088; Nucl. Phys. **B583**, 3 (2000).
[33] K. G. Chetyrkin, Nucl. Phys. **B710**, 499 (2005); arXiv:hep-ph/0405193 v3.
[34] J. C. Bloch, Few-Body Syst. **33**, 111 (2003).
[35] W. Celmaster and R. J. Gonsalves, Phys. Rev. D **20**, 1420 (1979).
[36] Ph. Boucaud, J. P. Leroy, J. Micheli, O. Pène, and C. Roisnel, J. High Energy Phys. 10 (1998) 017; arXiv:hep-ph/9810322.
[37] A. Maas, J. Wambach, and R. Alkofer, Eur. Phys. J. C **42**, 93 (2005); arXiv:hep-ph/0504019.